Time-dependent mean-field theory of the superfluid-insulator phase transition

Luigi Amico[1] and Vittorio Penna[2]
[1]*Departamento de Física Teórica de la Materia Condensada & Instituto ''Nicolás Cabrera,'' Universidad Autónoma de Madrid, E-28049 Madrid, Spain and Dipartimento di Metodologie Fisiche e Chimiche per l'Ingegneria, Facoltá di Ingegneria, Universitàà di Catania & INFM, viale A. Doria 6, I-95129 Catania, Italy*
[2]*Dipartimento di Fisica, Politecnico di Torino & INFM, Corso Duca degli Abruzzi 24, I-10129 Torino, Italy and Schrödinger Institute, Boltzmanngasse 9, A-1090, Wien, Austria*
(Received 4 August 1999; revised manuscript received 18 January 2000)

We develop a time-dependent mean-field approach, within the time-dependent variational principle, to describe the superfluid-insulator quantum phase transition. We construct the zero-temperature phase diagram both of the Bose-Hubbard model (BHM), and of a spin-S Heisenberg model (SHM) with the XXZ anisotropy. The phase diagram of the BHM indicates a phase transition from a Mott insulator to a compressibile superfluid phase, and shows the expected lobelike structure. The SHM phase diagram displays a quantum phase transition between a paramagnetic and a canted phases showing as well a lobelike structure. We show how the BHM and the quantum phase model (QPM) can be rigorously derived from the SHM. Based on such results, the phase boundaries of the SHM are mapped to the BHM ones, while the phase diagram of the QPM is related to that of the SHM. The QPM's phase diagram obtained through the application of our approach to the SHM, describes the known onset of the macroscopic phase coherence from the Coulomb blockade regime for increasing Josephson coupling constant. The BHM and the QPM phase diagrams are in good agreement with quantum Monte Carlo results, and with the third-order strong-coupling perturbative expansion.

I. INTRODUCTION

Phase transitions induced by thermal or quantum fluctuations have been studied in various mesoscopic systems. Examples are Josephson junction arrays (JJA's),[1] granular,[2] and short-length superconductors.[3] Such systems have two different critical temperatures T_1 and T_0 $(T_0<T_1)$. Below T_1, they possess finite domains in which the electrons form the Cooper pairs: In each domain the condensate is described by the Cooper pairs' wave function $\psi_j=\Delta e^{i\Phi_j}$ $(\Delta=|\psi_j|$ beeing related to the pair density) and the system is globally resistive because of the absence of phase coherence between the Cooper pairs.[4] Below T_0, the system may reach the macroscopic phase coherence (global superconductivity).

If the characteristic energy scale of the system is much smaller than $|\Delta|$, one can regard the Cooper pairs as true bosons[5] and the global superconducting phase transition can be studied by analyzing the critical behavior of strongly correlated bosonic models on a lattice.[6,7] These exhibit two characteristic energy scales: the hopping amplitude t which accounts for the boson kinetic energy, and the Coulomb repulsion U which is the electrostatic energy expense to make bosons spatially close. The Bose-Hubbard model (BHM) can describe the energetic competition between t and U. The global superconducting phase transition is controlled by the ratio t/U which is a measure of *quantum effects*. For $t\ll U$, the strong quantum fluctuations of Φ_j prevent the system from reaching the phase coherence for any value of the temperature. The condition $t\gg U$ entails the classical regime: The system undergoes a phase transition at a finite value of temperature T_0 that belongs to the D-dimensional XY model's universality class. Below T_0 the system is superfluid, while above T_0 it becomes resistive. If the Coulomb interaction is comparable with the kinetic energy then quantum fluctuations make T_0 vanish, and drive the $(T_0=0)$ superconductor-insulator (SI) phase transition. The latter has been studied in great detail both experimentally[8] and theoretically.[6] The superfluid phase is characterized by off-diagonal-long-range-order signaled by a nonvanishing order parameter $\Psi=\langle e^{i\Phi_i}\rangle$ (*macroscopic quantum phase coherence*). The insulating phase is incompressible and it is characterized by $\Psi=0$. In particular, due to the dimensional crossover, the SI phase transition belongs to $(D+1)$-XY model's universality class for commensurate bosons' densities, whereas it is mean-field-like away from such values.[7]

We recall that the number of bosons n_j (at each site j) is standardly considered to be canonically conjugated with Φ_j. This establishes a competition between the quantum fluctuations of n_j, and those of Φ_j's.[9]

In a recent paper[10] we formulated a time-dependent mean-field theory (TDMFT) of the BHM in order to investigate some aspects of the physical scenery just described. The TDMFT was based on factorizing slow/fast dynamics described by an effective form of the BHM Hamiltonian. The latter was derived within the time-dependent variational principle (TDVP) procedure, and relied on a picture of the system quantum state in terms of Glauber coherent states. In this approach the Hamiltonian degrees of freedom identified by construction with the parameters $z_j(\tau)$—τ is the real time—of coherent states $|z_j\rangle$, that is the expectation values $(\langle z_j|a_j|z_j\rangle)$ of the operators $a_j(a_j^+)$ describing at each site j the destruction (creation) of bosons.[11]

We revealed that quantum effects concerning the competition between the Coulomb term and the hopping term are embodied in the time dependence of the coherent-state parameters $z_j(\tau)$. The TDMFT involves a time-dependent, *lo-*

 ©2000 The American Physical Society

cal order parameter which is assumed to represent the slowly varying part of z_j, and plays the same role of ψ_j. In Ref. 10, we have shown that ψ_j has a time-independent amplitude which is the analog of Δ, and a time-dependent phase which is the analog of Φ_j. In particular, the phase's quantum fluctuations were described in terms of phase's time fluctuations.

The phase transition is signaled by a qualitative variation of the time behavior of the local superconducting order parameter. In spite of the approximations involved by the TDMFT, indeed our phase diagram shows a good agreement with quantum Monte Carlo (QMC) simulations[13] and strong-coupling perturbative expansion (SCPE).[14]

The purpose of this paper is to extend the TDMFT of the BHM developed in Ref. 10 both to the spin-S Heisenberg Model (SHM) and to the quantum phase model (QPM) for constructing their zero-temperature phase diagrams.[15] To this end we establish a rigorous mapping between the SHM, the BHM and the QPM based on the Holstein-Primakoff realization and the Villain realization of the spin algebra. In particular, we shall see that the existence of such a mapping is crucial to construct the phase diagram for the QPM within the TDMFT of the SHM. In this case, in fact, the explicit representation of the Hamiltonian in terms of coherent states is problematic[16] due to the Euclidean algebraic structure of the QPM's degrees of freedom.

In outline, the paper is organized as follows. In Sec. II, we introduce the three models we deal with, we illustrate some basic aspects of their algebraic structure, and describe their qualitative phase diagrams. Based on the TDMFT, we construct in Sec. III the SHM's phase diagram. The latter will be shown to describe the SI transition only in some interval of external magnetic fields. The discussion developed here will concern the SHM's phase diagram only for magnetic field in that range. The full description of the SHM's phase diagram will be reported elsewhere.[17] In Sec. IV we employ the program developed in Appendix A to recover the BHM phase diagram from the SHM one, and to obtain the quantum Josephson model's phase diagram from the SHM phase boundaries. In Sec. V we give our conclusions and further remarks. Appendix A is devoted to a procedure following which both the BHM and the QPM are obtained from the SHM. In Appendix B we apply the TDVP method to work out the semiclassical BHM Hamiltonian and its dynamical equations. Then we formulate the TDMFT and employ it to construct the BHM's phase diagram. After reviewing the basic properties of spin-generalized coherent states,[18] the TDVP method is implemented in Appendix C for the SHM. In Appendix D we derive the phase dynamics of the QPM as a perturbation of the SHM minimum energy configurations.

II. THE MODELS

A convenient starting point for introducing models that exhibit the SI phase transition is the BHM.[1] It represents a boson gas of identical charges hopping through a *D*-dimensional lattice whose Hamiltonian reads

$$H_{BH}=\sum_j\ [U(n_j-1)-\mu]n_j-\frac{t}{2}\sum_{\langle i,j\rangle}\ (a_i^\dagger a_j+a_j^\dagger a_i),\quad (1)$$

where the operators $n_i:=a_i^\dagger a_i$ count the number of bosons at the site i, and the annihilation and creation operators $a_i, a_i^\dagger$ obey the canonical commutation relations $[a_i,a_j^\dagger]=\delta_{ij}$. The set $\{\mathbb{1},a_i a_i^\dagger n_i\}$ is the basis generating at each site a Heisenberg-Weyl algebra h_4. Also, the parameters t,U of Eq. (1) are the hopping amplitude and the strength of the onsite Coulomb repulsion, respectively, while the chemical potential μ fixes the average number of bosons in each site.

The phase diagram of the BHM has been studied thoroughly by means of mean field[7] and variational[19] approaches as well as perturbative[14] and quantum Monte Carlo[13] techniques. At $t/U=0$, the minimum energy configuration is characterized by an integer number n of bosons at each site, and a finite energy gap $\mu=2U$ for the creation of particle-hole excitations. This reflects the Mott insulator (MI) behavior of such a phase which entails a vanishing compressibility. The MI regime survives (except for the degeneration points with $\mu=2nU$) when $t/U>0$, inside extended *lobes* attached to intervals $I(n)=[2(n-1)U,2nU]$ of the μ/U axis in the $t/U-\mu/U$ plane. Elsewhere, in the phase plane, the system exhibits a superfluid character, both compressible and independent from the filling.

At the lobe boundary the appearence of the superfluidity is announced by the vanishing of the energy gap between the states corresponding to n (or $n-1$) and $n+1$ (or n) particles (or holes). Also, at the critical points the variance $\Sigma^2(\Phi)$ of the phase of the superconducting order parameter is reduced *so much* as the quantum coherence can take place. Indeed, the Φ_i's quantum fluctuation survives also in the superfluid phase and they are rigorously vanishing $[\Sigma_i^2(\Phi)=0]$ only in the *classical limit* $t/U\to\infty$. These two features characterize the whole MI-SF phase boundary as well as the onset of the superfluid state.

The QPM is deeply related to the BHM. It is largely employed for the description of quantum JJA's in which the phases Φ_i of the superconducting order parameter are dynamically relevant, the fluctuations of the modulus Δ being negligible at low temperatures. Since among the islands of nanofabricated samples no Ohmic current flows and quasiparticle tunneling is actually negligible, the QPM Hamiltonian defined as

$$H_{QP}=\sum_{i,j}\ Q_i V_{ij} Q_j-\frac{E_J}{2}\sum_{\langle i,j\rangle}\ \cos(\Phi_i-\Phi_j),\qquad (2)$$

with $Q_i:=N_i-N_x$, can capture the physics of JJA's. In Eq. (2), N_i counts the number of Cooper pairs which make the island deviate from the neutrality state with respect to the background charge. The standard assumption that phase operators Φ_i are canonically conjugated to N_i's, namely $[\Phi_i,N_j]=2ei\delta_{ij}$, requires coherently that the N_i eigenvalues must range from $-\infty$ to $+\infty$. The Coulomb interaction is described by the matrix $V_{i,j}=4e^2(C^{-1})_{i,j}$, where $C_{i,j}$ is the inverse of the capacitance matrix. In the sequel we will assume $V_{i,j}=V\delta_{i,j}$ with $V\equiv 4e^2C_0^{-1}$, where C_0 is the self-capacitance. The external voltage $V_x\doteq N_x/V$ enters via the induced charge eN_x, and fixes the average charge on each island. The phase diagram of the QPM is similar to BHM's one (see Refs. 20,21). The MI lobes are attached to the interval $I(N_0)=[(N_0-1/2)V,(N_0+1/2)V]$, where the average number of Cooper pairs is $N_0\doteq int(N_x)$. The degeneration points at $E_J/V=0$ are $N_x=N_0/2$. Outside the lobes the system is globally coherent and exhibits a superfluid character.

The argument usually employed to map the BHM on QPM is heuristic: In the limit of large average number of boson per site the bosonic field may be represented as $a_j \simeq \sqrt{n_j} e^{i\Phi_j}$, $a_j^\dagger \simeq e^{-i\Phi_j}\sqrt{n_j}$ (Φ_j being Hermitian), where the operators $n_j \doteq N_j - N_x$ have negligible fluctuations, and play the role of Cooper pairs' density. The QPM is recovered through the identifications $N_x \equiv \mu/\Sigma_j U_{i,j}$ and $E_J \equiv nt$ (n is the average boson density). Since the fluctuations of n_j are underestimated in the QPM the superfluid region is smaller than the BHM one.

It is worthwhile noting how a rigorous reading of this mapping leads to severe inconsistencies.[16] These are mainly due to the boundness from below of bosonic number operators n_j that makes extremely complex the problem of defining the Hermitian phases canonically conjugated to n_j.[22] Nevertheless, the QPM can be defined in a consistent way since the operators $N_i := -i\partial_{\Phi_i}$, and $\exp(\pm i\Phi_i)$ with Φ_i an *Hermitian phase* are employed in formula (2).

The difficulties involved in mapping the BHM into the QPM in a direct way can be circumvented by using a third (spin) model as a bridge connecting the first ones. To this end we first describe the standard way to relate anisotropic spin-1/2 Heisenberg model with the physics of the SI transition, then we introduce the spin-S model that will be employed in the sequel.

At very low temperature, few charge states are important if on-site Coulomb repulsions are very large. If the gate voltage is tuned close to a degeneracy, two charge states per island actually suffice to represent the relevant physics. Therefore, the *hard core* BHM is equivalent to a spin-1/2 Heisenberg model (see Ref. 23) the model Hamiltonian of which is represented in terms of su(2) operators S_i^z, S_i^+, S_i^- in the fundamental representation. Substitutions $S_i^z \to n_i - 1/2$, $S_i^+ \to a_i^+$, and $S_i \to a_i$ allow one to recover the hard-core BHM from the spin-1/2 Heisenberg model.

The zero-temperature phase diagram of the spin-1/2 Heisenberg model has been investigated in Refs. 23,24 within the mean-field approximation. This shows the presence of a phase transition between paramagnetic/Néel phases in which $\langle S_i^z \rangle \neq 0$ and $\langle S_i^\pm \rangle = 0$, and a *canted* state in which $\langle S_i^z \rangle = \langle S_i^\pm \rangle = 0$.

Such magnetic orderings have a counterpart in the BHM's phases: the canted state (long-range order in $\langle S_i^x \rangle$ and $\langle S_i^y \rangle$) indicates superfluidity in the BHM; the paramagnetic/Néel phases (long-range order in $\langle S_i^z \rangle$: $|\langle S_i^z \rangle| \neq 0$) correspond to the MI's (the role of μ is played by the Heisenberg model external magnetic field h). The representation in terms of the (anisotropic) spin-1/2 Heisenberg model cannot work for the soft core BHM, this involving, in general, more than two charge states .

We propose the spin-S XXZ Heisenberg model (denoted so far by SHM) as a model capable of describing the physics of the SI phase transition when more than two charge states are involved. In this case the Hamiltonian has the form of the anisotropic spin-1/2 Heisenberg model, but (the representation index) $S > 1/2$. It reads

$$H_S = \sum_i (S_i^z + S)[U(S_i^z + S - 1) - h] - \frac{E_S}{2} \sum_{\langle i,j \rangle} (S_i^+ S_j^- + S_j^+ S_i^-), \tag{3}$$

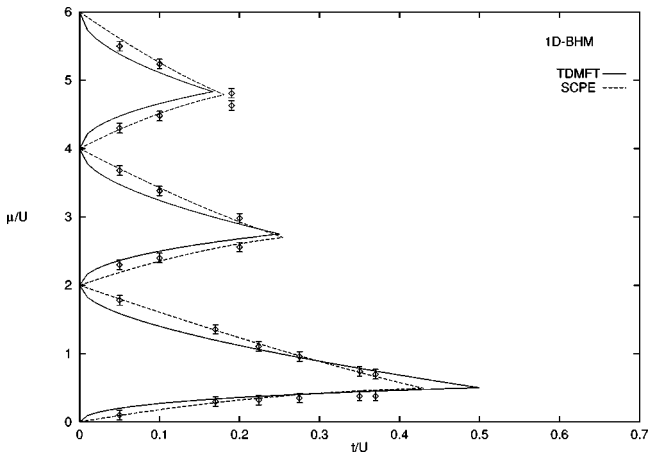

FIG. 1. The phase diagram of the BHM for $D=1$. The error boxes are the QMC results of *Batrouni et al.* in Ref. 13. The dashed lines are the result of the SCPE. Relatively to the first lobe ($n_i = 1$), Eq. (B24) gives $(t_c/U) = 0.5$. QMC gives $(t_c/U) = 0.43 \pm 0.002$ and the SCPE $(t_c/U) = 0.43$. For ($n_i = 3$), QMC and SCPE give $(t_c/U) = 0.2$ and $(t_c/U) = 0.18$, respectively. Our theory gives $(t_c/U) = 0.16$.

where we have taken into account only the on-site interaction along z. In Appendix A we describe a procedure which maps the SHM onto the BHM and the QPM.

III. TDMFT OF THE SHM

In this section we construct the phase diagram representing the SI phase transition for the SHM and compare it with that of the BHM represented in Figs. 1 and 2. We develop a construction, the main steps of which are very similar to the TDMFT of the BHM depicted in Appendix B; thus we will sketch them without comment when the analogy with the TDMFT of the BHM is evident.

The semiclassical SHM model is achieved by projecting Hamiltonian (4) on the su(2) coherent states (see Appendix B), thereby obtaining

$$\mathcal{H}_S = \sum_i (UL_i^z - h_*)L_i^z - \frac{E_S}{2} \sum_{\langle i,j \rangle} (L_i^* L_j + L_j^* L_i) + C, \tag{4}$$

where $h_* := h - U(2S-1)$, and $C := \Sigma_i S[h_* + U(S-1/2)]$. The semiclassical equations of motion obtained within the TDVP method[25] read

$$i\hbar \dot{L}_j = [U(2L_j^z + 2S - 1) - h]L_j + E_S L_j^z \sum_{i \in (j)} L_i. \tag{5}$$

Equations (5) are not integrable, since the constants of motion available are just two, namely the z component of the total angular momentum $L_z = \Sigma_j L_j^z$ and the energy itself. The TDMFT decoupling simplifies Eq. (5) through the approximation

$$L_i L_j^* \approx \mathcal{M}_i L_j^* + L_i \mathcal{M}_j^* - \mathcal{M}_i \mathcal{M}_j^*, \tag{6}$$

which ensues from $(L_i - \mathcal{M}_i)(L_j^* - \mathcal{M}_j) \approx 0$ and entails $\langle L_j \rangle_\tau = \mathcal{M}_j$ on long-time scales [compare with Eqs. (B7) and (B8)]. The order parameter is defined as

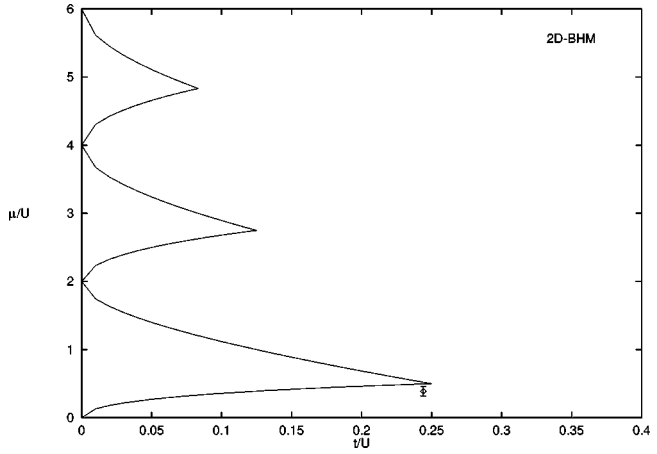

FIG. 2. The phase diagram of the BHM for $D=2$ (continuous curve). The error box indicates the QMC tricritical point obtained by *Krauth and Trivedi* in Ref. 13. For $n=1$, $(t_c/U)=0.25$ while QMC gives $(t_c/U)=0.244\pm0.002$ and SCPE provides $(t_c/U)=0.272$.

$$M\equiv\frac{1}{N_s}\sum_j\langle L_j\rangle_\tau. \tag{7}$$

When Eq. (6) is inserted in Eq. (4) together with the uniformity condition $\mathcal{M}_j\equiv\mathcal{M}\forall j$, Hamiltonian (4) reduces to a sum of on-site terms: $\mathcal{H}_S\rightarrow\Sigma_j\mathcal{H}_j$, where

$$\mathcal{H}_j=\text{const}+(UL_i^z-h_*)L_i^z - \frac{qE_S}{2}(\mathcal{M}_jL_j^*+\mathcal{M}_j^*L_j-|\mathcal{M}_j|^2). \tag{8}$$

The equations of motion derived from Eq. (8) simplify to

$$i\hbar\dot{L}_j=(2UL_j^z-h_*)L_j-qE_SL_j^z\mathcal{M}_j \tag{9}$$

and imply that L_z is no longer a constant of motion. In analogy to the BHM case of Appendix B, implementing the phase-locking condition $\phi_j-\alpha_j=\{0,\pi\}$ on $L_j=|L_j|e^{i\phi_j}$ and $\mathcal{M}_j=|\mathcal{M}_j|e^{i\alpha_j}$, $(\phi_j,\alpha_j\in[0,2\pi])$ successfully restores the basic feature $dL^z/dt=0$. Due to Eqs. (9) the phases ϕ_j obey the equation

$$-\hbar L_j\dot{\phi}_j=(2UL_j^z-h_*)L_j-qE_SL_j^z\mathcal{M}_j. \tag{10}$$

We examine first the spin dynamics related to the paramagneticlike phase. Such a phase is identified by $\langle S_j^z\rangle$, sharply peaked at one of its spectral values m: $\Sigma^2(S_i^z)\ll1$; this condition (due to the uncertainty principle) induces strong quantum fluctuations of S_j^x and S_j^y which suppress the ferromagnetic order in the $x-y$ plane. Semiclassically, $\Sigma^2(S_i^z)\ll1$ translates in $L_j^z=m$.

Within our scheme, the condition $L_j^z=m$, $\forall j$ follows from the requantization procedure[26,27] of the actionlike variables L_j^z (notice that $\{L_j^z,\phi_j\}=\delta_{ij}/\hbar$), and entails $|L_j|=\sqrt{S^2-m^2}$. Since Eq. (10) is solved by $\phi_j=\tau\rho_\pm/\hbar+\phi_j(0)$, then

$$\mathcal{M}_j=\pm\frac{U\Delta+\rho_\pm}{qE_SL_j^z}L_j. \tag{11}$$

We have parametrized the external magnetic field as $\Delta:=h_*/U-2m$. The parameter $\rho_+(\rho_-)$ is related to the choice $(\phi_j-\alpha_j)=0$ $[(\phi_j-\alpha_j)=\pi]$. The order parameter

$$M=\frac{1}{N_s}e^{i\tau\rho_\pm/\hbar}\sum_j\mathcal{M}_je^{i\phi_j(0)}$$

has a vanishing (long) time average $\langle M\rangle=0$, because of the time-dependent phase factor $e^{i\tau\rho_\pm/\hbar}$. Such a phase factor forbids the breaking of the so(2) rotational symmetry of the SHM in the xy plane. Thus, the oscillating behavior of M_j identifies the paramagnetic phase. Notice that the condition $\langle M\rangle=0$ can be realized also for $\mathcal{M}_j\neq0$: As in the case of the TDMFT of the BHM, the TDMFT of the SHM can describe the paramagnetic phase for $E_S>0$.

The frequencies $\rho_\pm$'s play the role of time correlation length governing the phase transition. The observations of Appendix A as to the criticality of BHM can be extended to model (3): As expected, the critical exponents z and ν fulfill the same Eq. (B16). The latter is left unchanged by the procedure mapping the SHM onto the BHM and QPM. Hence, this suggests that the same Eq. (B16) governs the criticality of the QPM.

Equation (11) play the role of the self-consistent equations of the TDMFT: They serve to eliminate the order parameter from the energy (8). The energy of the paramagnetic phase reads

$$\mathcal{E}_m(h,E_S;\rho)=-U(\Delta+m+S)(m+S) - \frac{2qE_Sm-\rho_\pm-U\Delta}{2qE_Sm^2}[U\Delta+\rho_\pm](S^2-m^2). \tag{12}$$

The condition $h_*/U-2m=0$ $(\Delta=0)$ identifies the degeneration points at which the canted phase reachs the axis $E_S/U=0$. The points on such an axis correspond to static solutions of the equation of motions (9) which are obtained through $\rho_\pm=0$. Such a condition is the simplified form of the low-frequency dynamics in the canted state.

Now, we consider the fixed points of the dynamical equations (9) that identify the canted phase. In such a case the self-consistent equations read

$$\mathcal{M}_j=\frac{h_*-2UL_j^z}{qE_SL_j^z}L_j. \tag{13}$$

The calculation of the energy minimimum of the canted phase is considerably simplified by applying the change of variable

$$p_j=\frac{h_*-2UL_j^z}{qE_SL_j^z}, \tag{14}$$

which implies that the self-consistency equation can be written as

$$\mathcal{M}_j=p_j\sqrt{S^2-\left(\frac{h_*}{qE_Sp_j+2U}\right)^2}. \tag{15}$$

After noting that the order parameter $\mathcal{M}_j$ is a monotonic (increasing) function of p_j we are allowed to eliminate the

order parameter from the energy (8) then minimizing it with respect to p_j. The energy reachs its minimum value at $p_j = 1$ which corresponds to

$$(L^z)_{\min} = \frac{h_*}{qE_S + 2U} \equiv \mathcal{L}_0, \tag{16}$$

where the index j has been dropped since the uniformity of the solution. We point out that setting $p_j = 1$ in Eq. (13) implies $\mathcal{M}_j = L_j$ on which the TDMF decoupling is based. The minimum energy is

$$\mathcal{E}_{\min} = U\frac{S}{2} - \frac{(h + qSE_S + U)^2}{2(qE_S + 2U)}. \tag{17}$$

Energy (17) gives the known (see Ref. 24) classical value of the energy minimum (up to the constant $US/2$, see Appendix B). Thus we conclude that the static solutions of Eq. (9) correspond to the classical canted phase.

Now we employ the energy (12) to obtain the phase boundaries between the paramagnetic and the canted phases. The curves representing the m-phase boundary are identified by implementing the so(2) symmetry breaking through the limits $\rho_{\pm} \to 0$ and the vanishing of the energy gaps $\mathcal{E}_m - \mathcal{E}_{m\pm1}$ [compare with Eqs. (B21) and (B22)]. In particular, $\mathcal{E}_m = \mathcal{E}_{m+1}$ provides the equation

$$\frac{U}{2qE_S}\Delta_-^2 - r_m\Delta_- + s_m = 0, \tag{18}$$

where $\Delta_- := h/U - 2(m+S) \leqslant 0$, and $r_m := m(m+1)/(1+2m)$, $s_m := [2(m+S)+1](1+2m)r_1^2/S^2$. A second equation is derived from $\mathcal{E}_m = \mathcal{E}_{m-1}$ where Δ_- must be replaced by $\Delta_+ := h/U - 2(m+S) + 2 \geqslant 0$. As in the bosonic case, the upper (lower) root issued from $\mathcal{E}_m = \mathcal{E}_{m-1}(\mathcal{E}_{m+1} = \mathcal{E}_m)$ gives the phase boundaries

$$\frac{h_+}{U} = 2(m+S-1) - \frac{qE_S m(m+1)}{U(2m+1)} \times \left[-1 + \sqrt{1 - \frac{2U}{qE_S S^2}(2m+1)[2(m+S)+1]}\right], \tag{19}$$

$$\frac{h_-}{U} = 2(m+S) - \frac{qE_S(m+1)(m+2)}{U(2m+3)} \times \left[-1 - \sqrt{1 - \frac{2U}{qE_S S^2}(2m+3)[2(m+S)+3]}\right]. \tag{20}$$

We study the phase diagram (19), (20) for $m < -1/2$. Such a restriction guarantees that the canted phase propagates up to $E_S/U = 0$ at the degeneration points $\Delta = 0$ for any value of $m < -1/2$ (otherwise the paramagnetic lobes meet one each other at $\Delta = 0$, but at $E_S/U \neq 0$). This feature is a common property of the phase diagrams which describes the SI transition. The above condition selects values of the external magnetic field h in the range $-2U < h < (S - 3/2)U$. Such a limitation will be relaxed in a forthcoming paper.[17] Figure 3 shows the phase diagram of the SHM for $S = 10$. We note

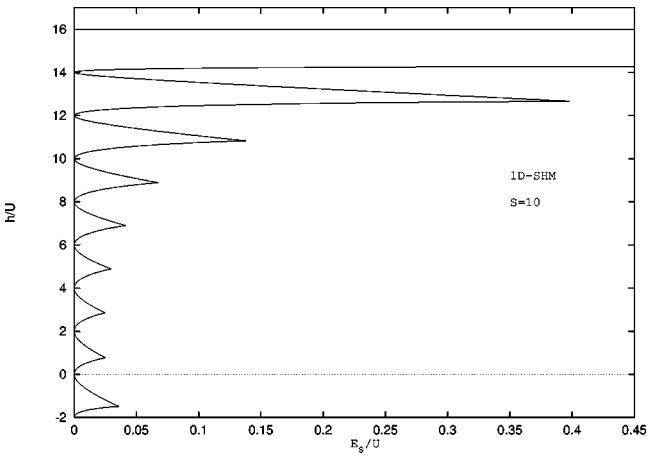

FIG. 3. The phase diagram of the SHM for $D = 1$ and $S = 10$. Inside the lobes the ground state is paramagnetic. Elsewhere the system is in a canted phase. The lobes are obtained for m ranging from $m = -S$ (corresponding to $-2 < h/U < 0$ in the figure) to $m = 1$ (the upset lobe). The coordinates E_S/U of the first two lobes' (corresponding to the $-2 < h/U < 2$ lobes) tricritical points decrease; they are ''almost'' constant for $0 < h/U < 4$ (named ''inversion region'' in the text). The SF phase is progressively reduced for increasing m (i.e., such that $4 < h/U < 16$).

that the coordinates $(E_S/U)_{tr}$ of the tricritical points (the cusps of the lobes) are not monotonic as a function of m (see also Fig. 5). In the lower part of the phase diagram they *decrease* monotonically (increasing m starting from its minimum value $-S, h = -2$ in Fig. 3) up to a critical value of m at which they are almost independent on m (we call the ''inversion region'' such a portion of the SHM phase diagram). In the lower part of the phase diagram, the shape of lobes is asymmetric. Instead, within the inversion region, the lobes are almost symmetric around odd-integer values of $m+S$. Increasing S makes especially wide the inversion region. In such a region we can assume the effects of the L^z's dynamics independent on m. For larger values of m $(E_S/U)_{tr}$ increases monotonically with m. Figure 5 shows the nonmonotonic behavior of the tricritical points for various values of S. In

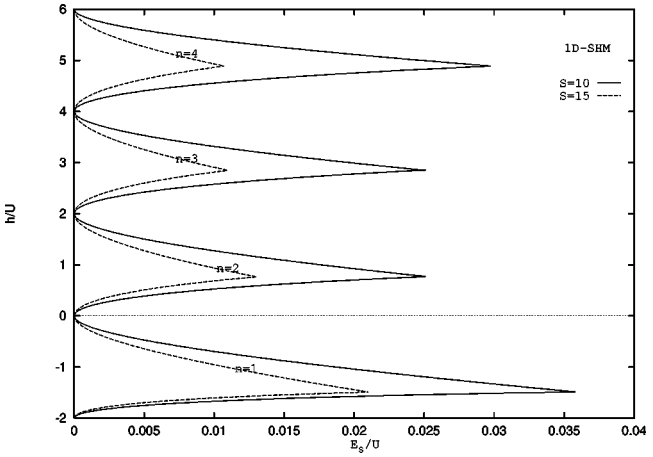

FIG. 4. The phase diagram of the one dimensional S-XXZ model for $S = 10$ and $S = 15$. The lobes are obtained for m ranging in $[-S, -1]$; in the figure, $n = m + S$ ranges in [1,4]. We note that the SF phase is enlarged for increasing S.

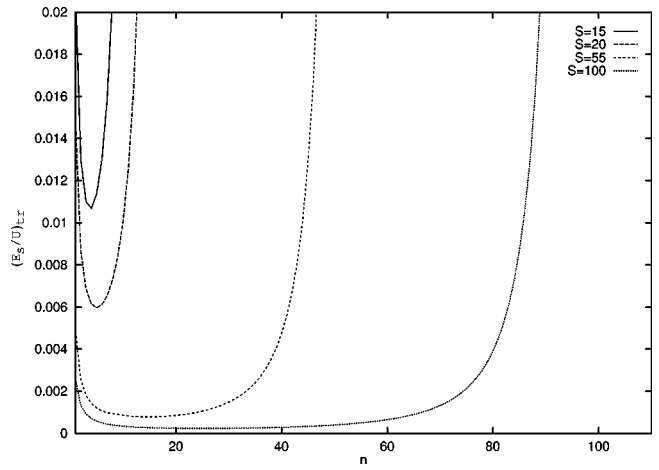

FIG. 5. The behavior of the tricritical points $(E_S/U)_{tr}$ as function of n for different values of S. We note that the region in which $(E_S/U)_{tr}$ is almost constant (named inversion region in the text) becomes wider for increasing S. Within this region the SHM's dynamics can be considerd as pure phase dynamics. This behavior is named ''QPM-like behavior'' in the text.

line with the mapping developed in Sec. III, in the next section we show that the SHM phase diagram contains the BHM (QPM) phase diagram in the lower (inversion) region.

IV. FROM THE SHM TO THE BHM AND QPM PHASE DIAGRAM

In this section we apply the results of Sec. III to construct the phase boundaries of both the BHM and the QPM from the phase diagram of the SHM.

We first recover the BHM phase diagram as a limiting case of the phase boundaries (19), (20) for $S \gg 1$, $\alpha \to 0$. The latter allows one to expand the energy of the paramagnetic phase (12) in power of α; upon relating the parameters E_S, h with t, μ as in Appendix A, we find that the energy of the paramagnetic phase (12) reduces to the form

$$\mathcal{E}_m(h,E_S;\rho_\pm)=E_n(\mu,t;\rho_\pm)-n\left[1+2\frac{\rho_\pm+U(\delta+1)}{qt}\right]\times[\rho_\pm+U(\delta+1)]\alpha+\mathcal{O}[\alpha^2]. \tag{21}$$

Such a formula shows that, at the zeroth order in α, $\mathcal{E}_m$ matches the on-site energy in the Mott phase (B17). In Fig. 6 we compare the phase diagram of the BHM with the SHM phase diagram worked out using the energy (12) for $S=55$.

Similarly, we can obtain the phase diagram of the QPM by taking the limit $S,m \gg 1$, $\beta^2 \ll 1$ of the phase boundaries (19), (20). As pointed out previously, we recall that a coherent states picture of QPM is not yet available in terms of coherent states of $e(2)$ [which is the algebra of the QPM microscopic degrees of freedom, see Eq. (A3)].[16] Hence, the direct application of the TDMFT, which relies on the coherent states description of the Hamiltonian operators, cannot be implemented in a direct way. The mapping outlined in Appendix A is crucial to bypass such difficulties. It allows, in fact, to construct the QPM phase diagram within the SHM lobelike structure provided the values of m/S remain inside a suitable range (see below). As stated in Appendix A, the

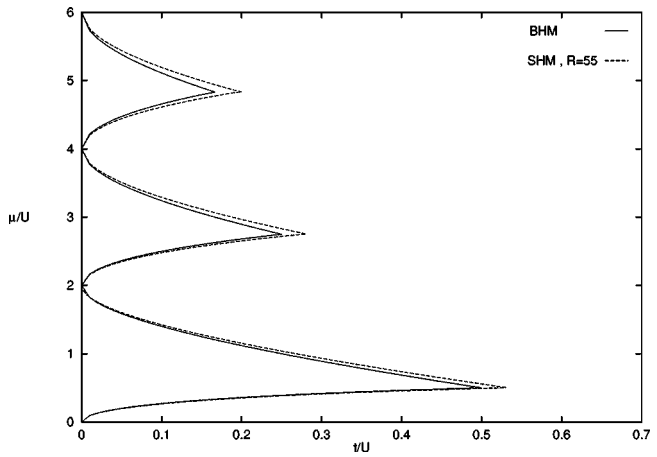

FIG. 6. The phase diagram of the BHM compared with the phase diagram of the SHM for $S=55$. The two phase diagrams coincide considering the zeroth order in α in formula (21) with $t=2SE_S$ and $h=\mu$.

condition $S \gg |m|$ together with the identifications $U \equiv V$, $N_x \equiv h_*/2U$, and $E_J \equiv S^2 E_S(1-\beta^2)$ recast the SHM Hamiltonian in the QPM form (see Appendix C). Correspondingly, the phase boundaries take the form

$$N_x^{\pm}=\frac{2m\mp 1}{2}+\frac{q\beta}{US}\left[E_J\mp\sqrt{E_J^2+8\frac{UE_J}{q}S^2\beta(1-\beta)}\right]. \tag{22}$$

We note that, for sufficiently large S, small changes of m leave the parameter β almost unaltered. This is sufficient to make the SHM phase diagram periodic in N_x. The curves (22) give a qualitatively correct QPM phase diagram for any $\beta^2 \ll 1$. We fix β in Eq. (22) to reproduce quantitatively the QMC phase diagram. Figures 7 and 8 show the phase diagram of the SHM model for $S=55$. The paramagnetic phases of the SHM turn in to the Coulomb blockade of the Cooper pairs. The canted state reveal the macroscopic phase coherence of the QPM.

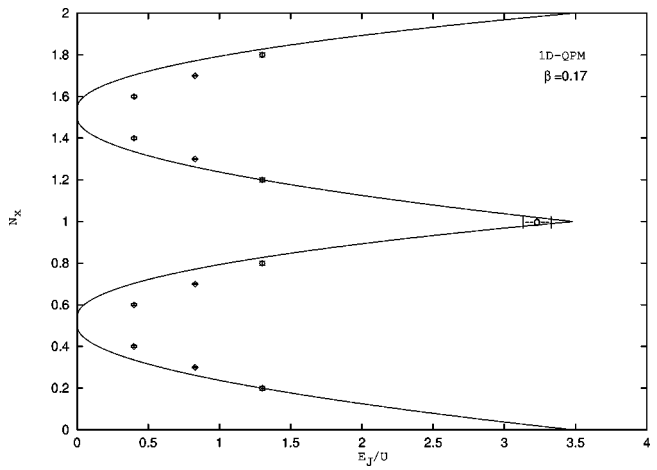

FIG. 7. The phase diagrams of the SHM for $S=55$ and $\beta=0.17$ in $D=1$. The errorbars are the result of the QMC simulations of the QPM of Ref. 36.

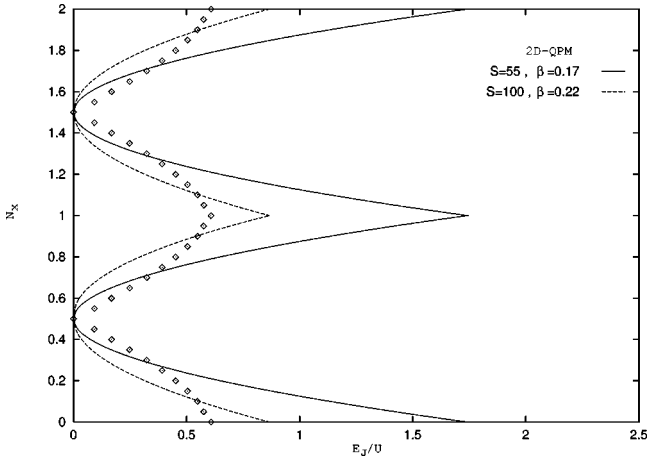

FIG. 8. The phase diagrams of the SHM for $S=55$ and $\beta=0.17$ and for $S=100$ and $\beta=0.22$ in $D=2$. The boxes are a result of QMC simulation of Ref. 37.

V. CONCLUSIONS

In this paper we have been concerned with two different aspects of the SI transition. The former is the algebraic structure that characterizes the main models exhibiting the SI phase transition. The latter is the development of the time-dependent mean-field theory (TDMFT) for the spin S Heisenberg model with XXZ anisotropy (SHM) that generalizes the approach previously elaborated for the Bose-Hubbard model (BHM). Remarkably, such a theory appears to be applicable to a large class of spin models.

The analysis of Appendix A concerning the algebraic framework in which the SHM is constructed, indicates that the correct way to map the SHM on the BHM is given by the Holstain-Primakoff realization of spin operators. Instead, the quantum phase model (QPM) is related to SHM through Villain's realization of the spin operators. Thanks to the transparent geometric meaning of such realizations[35,27] both the BHM and the QPM can be issued from the SHM by considering the appropriate sectors of the spin spectrum. To summarize: the BHM Hamiltonian emerges in the limiting case of spin vectors close to the south pole of the spin sphere, while the QPM behavior is found for spin vectors around the sphere equatorial plane.

The TDMFT have been presented in an extensive way in Appendix B, where it is used to investigate the BHM and its SI phase transition. Such a theory is based on combining the time-dependent variational principle (TDVP), the coherent state picture of the model quantum dynamics, the Einstein requantization procedure, and a time-dependent generalization of the mean-field decoupling.

The central assumption in our theory is that at $T=0$, time dependence of the semiclassical variables $z_i(\tau)$ represents the analog of the quantum fluctuations of operators a_i.

Although Eqs. (B5) (the semiclassical counterpart of Heisenberg's equations for a_j's) have been simplified to describe an on-site dynamics concerning z_j's, they furnish a consistent description of the system's quantum phase transitions. This is due to the semiclassical requantization procedure [see Eq. (B14)], on the one hand, and on the time dependence characterizing the phase of the superconducting order parameter, on the other. The latters make the order-parameter phase the main responsible in driving the SI transition. Within the TDMFT, we have established a relation between the dynamical behavior of the (local) superconducting order parameter and the macroscopic phases exhibited by the BHM. The Mott phase has been shown to be characterized by time fluctuations of the phase of the superconducting order parameter, whereas the superfluid phase is related to the static solutions of the (mean-field) equations of TDVP. The energy minimum coincides with the classical $t/U \gg 1$ superfluid case.

Below, we compare the ordinary MFA (mean-field approximation) with the TDMFT. The first comment in order is that the time-independent MFA of the BHM (Refs. 7,29) describes the SI phase transition by means of the suppression of the *amplitude* of the order parameter. The quantum fluctuations of the phase of the superconducting order parameter play no role in the standard MFA. Moreover, the MI phase is characterized by an on-site energy where the hopping term does not contribute.

The main difference between TDMFT and the standard MFA stands in the dynamical content of the definition of the superconducting order parameter: Within the TDMFT, the SF phase is suppressed by the (order parameter's) *phase*'s time fluctuations just as phase quantum fluctuations destroy macroscopic quantum coherence. Also, in the MI phase only the time average of the local parameters ψ_j is vanishing (along large time scale). This does not imply that ψ_j is strictly zero inside the insulator as it happens in the standard MFA. The good agreement with quantum Monte Carlo simulations and strong-coupling perturbative expansion confirms *a posteriori* that the superfluid phase is almost classical: Quantum fluctuations are strong in the insulating phase; they drive the SI phase transition, and are negligible in the superfluid phase, except in the regions very near to the phase boundaries.

Based on the introduction of the spin coherent states performed in Appendix C, the TDVP effective picture of quantum dynamics and the TDMFT of Appendix B have been extended to the SHM in Sec. III. Our analysis has revealed a quantum phase transition between a paramagnetic and a canted phase. The phase diagram exhibits a lobelike structure. Inside the lobes the phase is paramagnetic; elsewhere the system is in a canted state. The energy in the canted phase (represented by the stationary solutions of the equations of motions) coincides with the known classical energy.

We point out how the ordinary MFA [linearization of the xy exchange term in Eq. (3)] leads to study the reduced (on-site) Hamiltonian in the su(2) enveloping algebra [due to the $(S^z)^2$ term] which prevents one from diagonalizing the Hamiltonian for generic S.[30] Studying the spectrum of Eq. (3) for sufficently high S (which is done in the present paper) is in fact very problematic since the (matrix) Hamiltonian has a rank increasing with S. The classical analysis we have developed avoids such a problem and captures the lobelike structure of the SHM phase diagram.

The SHM's phase diagram contains the BHM's and QPM's ones. Using the strategy developed in Appendix A we have recovered the BHM energy as well as its phase diagram. As we pointed out previously, implementing the TDMFT to the QPM is problematic since the semiclassical description of the model in terms of the $e(2)$ coherent states

is not available. Nevertheless, the phase diagram of the QPM has been obtained as an appropriate limit (see Appendix A and IV) of the SHM phase diagram [the lobe structure is (locally) periodic around m for changes $m+\Delta m$ such that $\Delta m/S \ll m/S$]. This picture appears to be consistent with the QPM form assumed by the SHM (effective) Hamiltonian close to its ground-state configuration (see Appendix D), and suggests that possibly the (purely quantum) SHM can be reduced to the QPM form as well.

Other perspectives are opened by the present study.

First, the tools we used to map the SHM on the BHM and the QPM show how the enveloping algebra characterizing the BHM and QPM have common root in the enveloping algebra of the SHM. The mapping between these models can be seen as *contraction* procedure[31] of the enveloping algebras underlying the BHM, SHM, and QPM.[32] This suggests the fact that the universality class might be preserved by contraction.

Second, since the equations of motion (of the BHM and the SHM) obtained by the TDVP have been considered within the simplified form entailed by TDMFT, the dynamical approach refined out the TDMFT should imply a more accurate description of the superconducting order parameter dynamics as well as a better understanding of the low-temperature regime. As to this point, other improvements can be achieved by constructing trial wave functions able to account more accurately the microscopic physical processes (see Ref. 19). Finally, the TDMFT succeeds in capturing the main features of the quantum phase diagram of a rather large class of models. Promising applications of the TDMFT to other systems are expected due to its feasible character.

ACKNOWLEDGMENTS

The authors would like to thank L. Casetti, U. Eckern, G. Falci, R. Fazio, R. Franzosi, G. Giaquinta, R. Maciocco, A. Osterloh, M. Rasetti, and S. Sharov for valuable discussions. L.A. acknowledges financial suppport from EU TMR Program (ERB 4061 PL 95–0670), and the warm hospitality of the Theoretical Physics II in Augsburg. V.P. expresses his gratitude to the Schrödinger Institute in Wien, where part of this work was done, for supporting his visit as well as to the MURST for financial support within SINTESI Project.

APPENDIX A: MODEL MAPPING

In this appendix we give proof of the equivalence between the SHM, BHM, and QPM. The key operation of such a mapping consists in studying the model (3) for sufficiently high values of representation index S, and in using the Holstein-Primakoff realization (HPR) and the Villain realization (VR) of the spin algebra.

1. From the SHM to the BHM

We rewrite spin operators in Hamiltonian (3) by means of the HPR of the spin algebra su(2)

$$S_i^+ = \sqrt{2S}\, a_i^\dagger \sqrt{1-n_i/(2S)},$$

$$S_i^- = (S_i^+)^\dagger,$$

$$S_i^z = n_i - S, \tag{A1}$$

and note how, in view of the formulas of Appendix C, the eigenvalues of the secular equation for the ith spin $(S_i^z + S)|m_i,S\rangle = (m_i+S)|m_i,S\rangle$ ranging in $\{0,\ldots,2S\}$ identifies with the eigenvalues of n_i. Consistently, the spin states $|m_i,S\rangle$ coincide with the number operator eigenstates $|n_i\rangle$ up to the reparametrization $n_i = m_i + S$.

The condition $n_i/S \equiv (m_i+S)/S = \alpha \ll 1$ allows one to obtain Hamiltonian (1) from Eq. (3). In particular, the xy-exchange term of Eq. (3) gets in the hopping term of Eq. (1) with the hopping amplitude $t = 2(1-\alpha)SE_S \to 2SE_S$ for $S \to \infty$, and n_i finite. In the same limit, the spectrum of $S_i^z + S \equiv n_i$ ranges in $\{0,\ldots,\infty\}$ thus reproducing the spectrum of bosonic operators n_i. The z-antiferromagnetic term and the coupling with the external magnetic field term becomes the Coulomb interaction and chemical potential terms, respectively $(h=\mu)$.

Also, since $\alpha \equiv (m_i+S)/S$ (α has to be viewed as an order of magnitude independent on the site label i), the above limit corresponds quantum mechanically to select spin states close to lowest weight vector $|S,-S\rangle$ of the algebra $\mathrm{su}_i(2)$ (see Ref. 33) at the ith site. In this respect, we recall that, within the HPR, $|S,-S\rangle = |0\rangle$, where $a_i|0\rangle = 0$.

The effect of taking $\alpha \ll 1$ is illustrated by means of the semiclassical spin vector $\vec{L}$ (defined in Appendix C) lying on a sphere of radius S. Such a limit leads to select those vectors neighboring to the south pole of the sphere. Consistently, spin-coherent states $|\xi_i\rangle$ [see definition (C1)], that pertain to the Hilbert space of bosons within the HPR, can be shown to tend to the bosonic ones $|z_i\rangle$ for $\alpha \to 0$ [see Eq. (B2)], while the same limit makes the spin vectors on the sphere coincide, via stereographic projection, with the points of the south pole tangent plane.[34] These are in bijective correspondence with the complex numbers z_j labeling the bosonic coherent states. In fact, formulas (C3),(C4) clearly show that $L_j^z \to -S$ is achieved for negligible $|\xi_j|^2$ which also entails $L_j^* \to 2S\xi_j$, $L_j \to 2S\xi_j^*$. This in turn leads to the identifications $z_j^* \equiv L_j^*/\sqrt{2S} = \sqrt{2S}\xi_j$, $z_j \equiv L_j/\sqrt{2S} = \sqrt{2S}\xi_j^*$, and makes coincide brackets (C7) with brackets (B6). Hence the limit described above for the Hamiltonian operators is consistently reproduced at the classical level. We see in Sec. VI that the SHM phase diagram matches the BHM phase diagram for $\alpha \to 0$.

2. From the SHM to the QPM

We write the spin operators in Hamiltonian (3) by means of the Villain realization of su(2).[35] This is based on the formulas

$$S_j^+ = e^{i\phi_j}\sqrt{(S+1/2)^2 - (S_j^z+1/2)^2},$$

$$S_j^- = (S_j^+)^\dagger. \tag{A2}$$

Such operators fulfil the su(2) commutation rules provided the action-angle operators S_j^z, ϕ_j, satisfy the e(2) commutators

$$[S_l^z, e^{\pm i\phi_j}] = \pm \delta_{j,l} e^{\pm i\phi_j}, \quad [e^{i\phi_j}, e^{-i\phi_l}] = 0. \tag{A3}$$

The QPM (2) is obtained as a limiting model from Hamiltonian (3) when considering the first order in $\beta = |m_i|/S \ll 1$ for $S \gg 1$. The ferromagnetic part of Eq. (3) reduces to the Josephson term with coupling $E_J \equiv (S+1/2)^2 E_S(1-\beta^2)$ which in the limit $S \to \infty$ becomes $E_J \equiv S^2 E_S$. As in the case of α, the parameter $\beta = |m_i|/S$ must be regarded as a site-independent order of magnitude. Consistently, the spectrum of S_i^z will range from $-\infty$ to $+\infty$ thus reproducing the spectrum of the unbounded operator N_i in Eq. (2). The rest of Hamiltonian (3) maps to the charging term of Eq. (2) provided $V \equiv U$, and $N_x = [h + U(1-2S)]/2U$. It results $H_S \to H_{QP} + C_0$, where $C_0 = -(U+h)^2/4U$.

Geometrically, $\beta \ll 1$ amounts to selecting vectors neighboring the equatorial xy plane of the semiclassical sphere of radius S. This is well illustrated via formulas (C3), (C4) that provide $|\xi_i|^2 - 1 \ll 1 (|L_i^z| \ll S)$ as a counterpart of the above condition $\beta \ll 1$. Consistently, the sphere equation $(L_i^z)^2 + |L_i^*|^2 = S^2$ shows that $|L_i^*|^2 \simeq S^2$. Since both the Josephson coupling and the hopping amplitude contain the factor E_S, the formula $E_J = tS/2$ holds for $1 \ll S, \alpha \ll 1$, $\beta \ll 1$. Thus S plays the role of the boson density n (see Sec. II). We point out that the effective hopping coupling in the BHM is reduced by a factor S when compared with the Josephson coupling in QPM; consistently, the SF region of the BHM's phase diagram is smaller than the SF region of the QPM's one.

We note how, when considering the perturbative dynamics around the ground-state configuration of the SHM (see Appendix C), one obtains a QPM-like behavior (that is, having a pure phase's dynamics) without performing the limit $S \to \infty$. We see that the phase diagram of the QPM is obtained for $\beta^2 \ll 1$.[36]

APPENDIX B: THE TDMFT OF THE BHM

In this appendix we apply the TDVP (see Refs. 25 and 18 for a general review) to the quantum dynamics of Hamiltonian (1), and implement the TDMFT for the BHM.

1. Time-dependent mean-field theory

The initial step of the TDVP method amounts to finding a solution of the Schrödinger problem $(i\hbar\partial_\tau - H)|\Psi\rangle = 0$ by approximating the exact (unknown) solution $|\Psi\rangle$ through a macroscopic state $|\Phi\rangle$ whose time evolution is imposed to obey the weaker form of Schrödinger's equation $\langle\Phi|(i\hbar\partial_\tau - H)|\Phi\rangle = 0$. Upon setting $|\Phi\rangle = \exp(i\mathcal{S}/\hbar)|Z\rangle$ one obtains

$$\dot{\mathcal{S}} = i\hbar\langle Z|\partial_\tau|Z\rangle - \mathcal{H}(Z), \tag{B1}$$

$[\mathcal{H}(Z) \equiv \langle Z|H|Z\rangle]$, which represents the key equation of the approach.

The building blocks of Hamiltonian (1) are operators of the N_s-site Heisenberg-Weyl algebra $h_4(N_s) = \{\mathbf{I}, a_i, a_i^\dagger : i \in \Lambda\}$, N_s is the number of sites of the lattice Λ, but actually belongs to the enveloping algebra $\mathcal{A}$ of $W(N_s)$ because of the quadratic terms n_j^2. This motivates the choice $|Z\rangle := \otimes_j |z_j\rangle$ as the trial macroscopic state, entailing

$$|\Phi\rangle \equiv e^{i\mathcal{S}(\tau)/\hbar} \otimes_i |z_i\rangle, \tag{B2}$$

where the states $|z_i\rangle$ are the Glauber coherent states fulfilling the secular equation $a_i|z_i\rangle = z_i|z_i\rangle$ for the boson lowering operator a_i, at each site i. In this case the effective Lagrangian (B1) becomes

$$\dot{\mathcal{S}}[Z] = i\hbar \sum_i \frac{1}{2}(\bar{z}_i \dot{z}_i - \dot{\bar{z}}_i z_i) - \mathcal{H}(Z), \tag{B3}$$

where $\mathcal{H}(Z) = \langle Z|H|Z\rangle$—the semiclassical model Hamiltonian — is given by

$$\mathcal{H} = \sum_i (U|z_i|^2 - \mu)|z_i|^2 - \frac{t}{2}\sum_{\langle i,j\rangle} (\bar{z}_i z_j + \bar{z}_j z_i). \tag{B4}$$

The equations obtained variationally from Eq. (B3)

$$i\hbar\dot{z}_i = -\mu z_i + 2U z_i |z_i|^2 - \frac{t}{2}\sum_{j\in(i)} z_j \tag{B5}$$

account for the dynamics of variables (expectation values) $z_i = \langle z_i|a_i|z_i\rangle$. Equations (B5) describe a Hamiltonian flow in that they can be equivalently obtained through the standard formulas $i\hbar\dot{z}_j = \{z_j, \mathcal{H}\}$, where the Poisson brackets

$$\{f(Z,\bar{Z}), g(Z,\bar{Z})\} = \frac{1}{i\hbar}\sum_j \left(\frac{\partial f}{\partial z_j}\frac{\partial g}{\partial \bar{z}_j} - \frac{\partial g}{\partial z_j}\frac{\partial f}{\partial \bar{z}_j}\right), \tag{B6}$$

specifically, $\{z_k, \bar{z}_j\} = \delta_{kj}/i\hbar$ have replaced the basic commutators $[a_i, a_j^\dagger] = \delta_{ij}$ within the TDVP semiclassical framework. Equations (B5) are not integrable, since the only known constant of motion, apart from the energy, is $\mathcal{N} = \Sigma_i |z_i|^2$, i.e., the semiclassical version of the total particle number $N = \Sigma_i n_i$. The presence of the nonlinear U-dependent term prevents one from decoupling them in the dual lattice space.

The TDMFT procedure is, in a sense, the analog in a dynamical contest of the mean-field approximation (MFA) usually employed in statistical mechanics and is based on a well known microscopic picture of superfluids illustrated, e.g., in Ref. 37. It leads to simplifying the structure of Eqs. (B5). We set at each site $z_i = \psi_i + \eta_i$, where ψ_i is a slow variable, whereas η_i is a fast oscillating term which describes the high-frequency part of the dynamics taking place on the hopping interaction time scale. Also, we assume that $(z_i - \psi_i)(\bar{z}_j - \bar{\psi}_j) = \eta_i \bar{\eta}_j \approx 0$. Thus $\psi_j \equiv \langle z_j\rangle_\tau$ when the time scale τ is larger than that of the b_j's ($\langle\bullet\rangle_\tau$ denotes the time average). Such time averages coincide with statistical averages (in the Gibbs ensemble) under the ergodic assumption. The onset to the (macroscopically) ordered phase reflects the presence in the system of stable, slowly varying components of the lattice dynamics corresponding to the ψ_j's. This means that any z_j is strongly attracted to its average value ψ_j (namely that the collection of ψ_j's defines the dynamical system's attractor). Dynamical regimes where the long scale-time behavior of z_j is not described by an asymptotic slowly

varying function ψ_j is related with the disordered phases of the system. The above considerations imply the TDMF decoupling

$$z_i\overline{z_j} \equiv (z_i-\psi_i)(\overline{z_j}-\overline{\psi_j})+\psi_i\overline{z_j}+\overline{\psi_j}z_i-\psi_i\overline{\psi_j} \approx \psi_i\overline{z_j}+\overline{\psi_j}z_i-\psi_i\overline{\psi_j}. \quad \text{(B7)}$$

The dynamical scenery just depicted leads thus naturally to defining

$$\Psi \equiv \frac{1}{N_s}\sum_j \langle z_j\rangle_\tau \quad \text{(B8)}$$

as the macroscopic order paramenter revealing when order issues from the the lattice dynamics. Using formula (B7) in $\mathcal{H}$ modifies the kinetic term as follows:

$$\frac{t}{2}\sum_{\langle i,j\rangle}(\overline{z_i}z_j+\overline{z_j}z_i) \to \frac{qt}{2}\sum_i (\overline{z_i}\psi_i+\overline{\psi_i}z_i-|\psi_i|^2), \quad \text{(B9)}$$

where $\psi_j \equiv \psi_i$ for $j\in(i)$ (smoothing condition). The resulting Hamiltonian reduces to the decoupled form $\mathcal{H}_{mf}=\Sigma_j\mathcal{H}_j$, where

$$\mathcal{H}_j = U|z_j|^4-\mu|z_j|^2-\frac{qt}{2}(\overline{z_j}\psi_j+\overline{\psi_j}z_j-|\psi_j|^2), \quad \text{(B10)}$$

and exhibits a dimensionality dependence entering via the numbers of nearest neighbors q. The (decoupled) equations of motion ensuing from $\mathcal{H}_{mf}$ read

$$i\hbar\dot{z}_i = -\mu z_i+2Uz_i|z_i|^2-\frac{qt}{2}\psi_i. \quad \text{(B11)}$$

When compared with the exact ones, Eq. (B5), they imply the relation $q\psi_i \approx \Sigma_{j\in(i)}z_j$ consistently leading to an identity once the time average is carried on and the smoothing conditions is used. A further effect coming from the linearization (B9) consists in the fact that the total particle number $\mathcal{N}=\Sigma_i|z_i|^2$ does not have any longer vanishing Poisson brackets with $\mathcal{H}_{mf}$. Restoring such a basic feature is performed by considering z_j with an appropriate time dependence. To this purpose we look for solutions of Eqs. (B11) where θ_j,χ_j, the phases of

$$z_j=|z_j|e^{i\theta_j}, \quad \psi_j=|\psi_j|e^{i\chi_j}, \quad \text{(B12)}$$

respectively, obey the phase-locking condition $(\theta_j-\chi_j)=\{0,\pi\}$. Then $\mathcal{N}$ is constant due to the fact that $d|z_j|^2/dt=iqt(z_j\overline{\psi_j}-\overline{z_j}\psi_j)/2=0$. Moreover, the further condition $d|\psi_j|/dt=0$ consistently makes $\mathcal{H}_{mf}$ constant as expected for the total energy.

Due to Eq. (B11), the phase θ obeys the equation

$$-\hbar|z_j|\dot{\theta}_j=(2U|z_j|^2-\mu)|z_j|-s\frac{qt}{2}|\psi_j|, \quad \text{(B13)}$$

where $s=\pm$, depending on how the phase-locking constraint is implemented. In spite of its simplicity, such an equation is able to characterize both the MI phase and the superfluid phase in terms of phase dynamics.

We examine first the dynamics related to the MI. In this case, ψ_j must have a zero time average along macroscopic time scales. Such a behavior occurs when the uniform filling conditions $n_j=n$, for all i (we identify here number operators n_j's with their integer spectral values) is inserted in Eq. (B13) by setting

$$|z_j|^2=n\in\mathcal{N}. \quad \text{(B14)}$$

Such a substitution is the natural consequence of the requantization process[26,27] of the actionlike variables $|z_j|^2$ (notice that $\{|z_i|^2,\theta_j\}=\delta_{ij}/\hbar$) strongly requested from the pure quantum character of the MI. At $t/U=0$, where the system is integrable (since it reduces to a set of uncoupled, nonlinear oscillators) indeed θ_j and $|z_i|^2$ represent the pairs of action-angle variables of the system. For small values of t/U such a feature is still true as a consequence of the fact that the nonlinear oscillators are weakly interacting in the MI regime. Hence, in the spirit of Einstein's requantization procedure (see Ref. 26), their orbits are still homotopic to those of the integrable case which entails again $|z_j|^2=n$.

Equation (B13) is easily showed to be solved by $\theta_j(\tau)=\lambda_\pm\tau/\hbar+\theta_j(0)$, with $\lambda_\pm$ defined through

$$|\psi_j| \doteq \pm\frac{2\sqrt{n}}{qt}(\lambda_\pm-U\delta). \quad \text{(B15)}$$

Here we have parametrized the chemical potential as $\delta=\mu/U-2n$, and λ_- (λ_+) is related to the choice $\theta_j-\chi_j=\pi$ $(\theta_j-\chi_j=0)$ (notice that the index j does not label $\lambda_\pm$ since the request $\langle z_j\rangle_\tau\equiv\psi_j(\tau)$ leads to $|\psi_j|=\sqrt{n}$ at each site). In the present theory, the frequencies $\lambda_\pm$ play the role of time correlation length governing the phase transition. Our theory gives $\lambda_\pm=U\sqrt{n}(\mu-\mu_c)$ for fixed t and $\lambda_\pm=q|\psi_i|/2(t-t_c)$ for fixed μ (μ_c and t_c are the critical values of μ and t). Upon defining the critical exponents z and ν as in Ref. 7, we argue that[28]

$$z\nu=1. \quad \text{(B16)}$$

By replacing in the reduced Hamiltonian (B10) the value of $|\psi_i|$ provided by Eq. (B15), the energy of the MI reads

$$E_n(\mu,t;\lambda_\pm)=n\left[\frac{2}{qt}(\lambda_\pm+U\delta)^2+U(\delta-n)-2\lambda_\pm\right], \quad \text{(B17)}$$

where the subscript n reminds us that the filling n is accounted for. The oscillating behavior of $\Psi=(e^{i\tau\lambda_\pm}/N_s)\Sigma_j\psi_je^{i\theta_j(0)}$, having a vanishing long-time average, identifies the MI. This, in fact, implies that the gauge symmetry breaking expected in the SF phase cannot take place. Notice that the ordinary (time-independent) MFA cannot describe the MI for $t>0$, since the hopping term of the reduced Hamiltonian is canceled by the vanishing of the order parameter, $\psi=0$. Within our scheme, instead, the condition $\langle\Psi\rangle_\tau=0$ can be realized also for $\psi\neq0$. The degeneration points selected by $\mu/U=2n$ [i.e., $\delta=0$ in $I(n)$] are extreme limiting points for which the superfluid phase is extended up to $t/U=0$. They will be identified with the meeting points of the lobe boundaries. Such points characterize a static phase due to $\lambda_\pm=0$ [see Eq. (B13]. We interpret the stationarity which distinguishes the solutions of the semiclassical equation of motion as the trait characterizing the SF phase in which $\Sigma^2(\theta)=0$ (classical SF). This is but

the oversimplified version of the low-frequency dynamics expected in the SF phase that should correspond to the condition $\Sigma^2(\theta) \ll 1$.

Let us consider the fixed points of dynamical equations (B11) that, as we concluded above, identify the classical SF phase. Such solutions (the trivial case $\dot{z}_j = 0$ due to $z_j = \psi_j = 0$ is excluded) allow us to recast Eq. (B11) in the form $\psi_j = 2[(2U|z_j|^2 - \mu)/qt]z_j$ making ψ_j a function of z_j. Inserting $\psi_j(z_j)$ in Eq. (B10) reduces the energy associated to the Hamiltonian $\mathcal{H}_j$ to

$$\epsilon(\mu,t,z_j) = |z_j|^2 \left[\frac{2}{qt}(\mu - 2U|z_j|^2)^2 + \mu - 3U|z_j|^2 \right]. \tag{B18}$$

The quantity $\epsilon(\mu,t,z_j)$ is the on-site energy accounting for the absence of dynamics. The limit $\lambda_\pm \to 0$, in fact, shows that $E_n(\mu,t;\lambda_\pm) \to \epsilon(\mu,t,z_j)$ provided $n = |z_j|^2$. The lowest value of energy (B18) and the value z_* involved for z_j are obtained by minimization. They are given by

$$\epsilon_* = -U|z_*|^4 = -\frac{(\mu + qt/2)^2}{4U}, \tag{B19}$$

$$|z_*|^2 = \frac{(\mu + qt/2)}{2U}, \tag{B20}$$

respectively. The phase of z_* can be set to zero since the gauge symmetry-breaking characterizing the ground-state configuration. It is worth noting that inserting $|z_*|$ in the expression $\psi_j(z_j)$ implies that $\psi_j \equiv z_j$ so that the minimum energy configuration naturally fulfills the consistency condition on which our TDMFT is based.

Now, we employ the expression (B17) for the on-site energy to construct the BHM's phase diagram. In the SF phase, the states with n and $n+1$ (adding a particle), as well as the states with $n-1$ and n (adding a hole) must be degenerate. The curves representing the n-lobe boundary are identified by implementing both gauge symmetry breaking through the limits $\lambda_\pm \to 0$ and the vanishing of the energy gaps $E_n - E_{n\pm1}$. In other words we require

$$\lim_{\lambda_+ \to 0} (E_n - E_{n+1}) = 0 \quad (\delta < 0), \tag{B21}$$

$$\lim_{\lambda_- \to 0} (E_{n-1} - E_n) = 0 \quad (\delta > 0). \tag{B22}$$

For solving Eqs. (B21) and (B22) we introduce the variables $\delta_\pm = \mu/U - 2n + (1 \pm 1)$. By inserting $\delta_+ \geqslant 0$ ($\delta_- \leqslant 0$) in Eq. (B21) [(B22)], and defining $r = qt/4U$, one gets the quadratic equations $\delta_\pm^2 + 2r\delta_\pm - (2n \mp 1) = 0$, that furnish the pair of two-branched curves

$$\frac{\mu_\pm}{U} = 2n - 1 \mp 1 - \frac{qt}{4U}\left[1 \mp \sqrt{1 + \frac{8U}{qt}(2n \mp 1)} \right]. \tag{B23}$$

The lower branch $\mu_+(t)$ and the upper one $\mu_-(t)$ constitute the boundary encircling the nth lobe. The substitution of $\mu_-(t)$ and $\mu_+(t)$ in Eqs. (B21) and (B22), respectively, provides the on-site energy values involved in the two cases, namely $E_{n-1}(\mu_1,t) = E_n(\mu_1,t) = Un(n-1)$ and $E_n(\mu_2,t) = E_{n+1}(\mu_2,t) = Un(n+1)$. The two branches are, therefore, separated by an energy gap. Thus, the lobe tips are singular points of the energy. Their coordinates, obtained imposing $\mu_-(t) = \mu_+(t)$, reads

$$t_c = U/qn \tag{B24}$$

and $\mu(t_c)/U = 2n - 1 - (1/2n)$. The values of t_c obtained within the present theory, can be compared with QMC and SCPE (Ref. 14) (Figs. 1 and 2). Contrary to the result obtained in Ref. 14, our phase diagram has a concavity independent of the dimensionality. In 1D we find a good agreement with QMC and SCPE. Upon recalling that our construction relied on Eq. (B11)—this incorporates the time-dependent mean-field approximation—it is important to note that the concavity of lobes in $D \geqslant 2$ might be improved by implementing the requantization process directly on the Eqs. (B5).

2. Remarks on the SF ground state

As to the effectiveness of the approach just illustrated, two important observations are in order. The first is that our finding Eqs. (B19) and (B20) concerning the ground-state configuration is remarkably confirmed by two other procedures. The other concerns the macroscopic phase at the phase transition [see Eqs. (B27) and (B28)].

The minimum energy of the SF phase can be calculated from Eq. (B4). It represents the exact value of the BHM ground-state energy in the classical limit $t/U \gg 1$. The minimum energy is readily obtained by rewriting first the hopping terms as $(\overline{z_i} z_j + \overline{z_j} z_i) = |z_i|^2 + |z_j|^2 - |z_j - z_i|^2$, and by noticing then that the choice $z_l = \xi$ for each site entails the lowest value of the hopping term since the only positive contribution $|z_j - z_i|^2$ vanishes on each bond. Upon minimizing the resulting expression of the energy

$$\mathcal{H}_* = N_s \left[(U|\xi|^2 - \mu)|\xi|^2 - \frac{tq}{2}|\xi|^2 \right], \tag{B25}$$

by setting $d\mathcal{H}_*/d|\xi| = 0$, one obtains $|\xi|^2 \equiv (\mu + qt/2)/2U$ that matches exactly Eq. (B19): The ground-state energy (B18) coincides with the minimum of the exact (semiclassical) energy. Our approximation scheme thus reproduces the correct value of ξ as well as the corresponding value of the ground-state energy.

The ground-state energy eigenvalue can also be obtained once the Hamiltonian operator (1) is linearized via the standard procedure $n_j^2 \approx 2\nu n_j - \nu^2$, which is realiable for $t \gg U$. This yields the diagonalized Hamiltonian

$$H_{BH} \simeq -UN_s\nu^2 + \sum_k [2U\nu - \mu - tg(k)] b_k^+ b_k, \tag{B26}$$

when the operators $b_k = N_s^{-1/2} \Sigma_j a_j \exp[i\tilde{k}j]$ of the k modes are used. We have introduced $g(k) = \Sigma_r \cos(k_r)$ ($r \in [1,D]$ on a D-square lattice) where k_r is the rth component of $\vec{k}$. Hamiltonian (B26) clearly shows that its lowest eigenvalue is obtained through the depletion of any mode $k \neq 0$ (boson condensation in the state with $k = 0$). As a consequence of

the consistency condition $\langle n\rangle \equiv \nu (\Rightarrow N = N_s \nu)$, once more the energy is minimized by $\nu \equiv (\mu + qt/2)/(2U)$.

A comparison with the quantum ground-state energy—known exactly in the case $t/U=0$—is important as well. For $\mu/U \in I(n)$ the eigenvalues of H_{BH} with integer filling $n = N/N_s$, $E(\{n_j\}) = \Sigma_j [U n_j^2 - (\mu + U) n_j]$ reach their minimun value $E_* = -UN_s n^2$ for $n_j = n$ and $\mu/U = 2n-1$. The on-site energy $\epsilon_* = -U|z_*|^4$ [see Eq. (B20)] is found to attain exactly its quantum counterpart $E_*/N_s = -Un^2$ in the limit $t/U \to 0$, $\mu/U \to 2n$, namely at the point of $I(n)$ representing its top.

The second observation pertains to the action $\mathcal{S}$ that represents the phase of the macroscopic state $|\Phi\rangle$. It raises a special interest since it is itself a macroscopic quantity and thus is viable to experimental observations. In the following we compare $\mathcal{S}$ with $\mathcal{S}_{mf}$ (i.e., $\mathcal{S}$ in our TDMFT) as well as $\mathcal{S}_{mf}$ in the MI with $\mathcal{S}_{mf}$ in the SF.

When Eqs. (B5) are inserted in Eq. (B3) then $\dot{\mathcal{S}}$ reduces to

$$\dot{\mathcal{S}} = U \Sigma_j |z_j|^4, \tag{B27}$$

where the explicit form of $z_j(\tau)$ is known only once Eqs. (B5) have been really solved.

Inserting Eqs. (B11) instead of Eq. (B5) in Eq. (B3), and replacing $\mathcal{H}$ with its mean-field version $\mathcal{H}_{mf}$, involves

$$\dot{\mathcal{S}}_{mf} = \Sigma_j [U|z_j|^4 + t(\overline{z_j}\psi_j + \overline{\psi_j} z_j) - 2t|\psi_j|^2]. \tag{B28}$$

If $z_j \approx \psi_j$, then $\dot{\mathcal{S}}_{mf}$ and $\dot{\mathcal{S}}$ have essentially the same form. Such macroscopic quantities may actually coincide at the low-temperature regime if the dynamics of both $\mathcal{H}_{mf}$ and $\mathcal{H}$ have solutions characterized by $|z_j(\tau)|^2 \approx$ const. Within the present TDMFT $\dot{\mathcal{S}}_{mf} \equiv \dot{\mathcal{S}}$ since the condition $\eta_i \overline{\eta_j} \approx 0$ implies $z_j \approx \psi_j$; furthermore, $|z_j(\tau)|$ is strictly time independent.

In the MI the requantization rule (B14) must be used. The frequency $\dot{\mathcal{S}}_{mf}$ is obtained from Eq. (B28) by inserting Eq. (B14). $\mathcal{S}_{mf}$ reads as

$$\dot{\mathcal{S}}_{mf} = UN_s n^2. \tag{B29}$$

A transition that changes the filling from n to $(n+1)$ involves a change of the phase frequency amounting to $UN_s(2n+1)$. The action density in the superfluid phase reads $\dot{\mathcal{S}}_{mf} = UN_s|z|^4$, which compared with the corresponding formula (B29) shows that the frequency is not quantized. In the SF phase transitions between different configurations (different values of the filling) occur continously.

APPENDIX C: SPIN-COHERENT STATE PICTURE OF *XXZ* MODEL

Spin-coherent states (SCS) $|\xi\rangle$ are defined as

$$|\xi\rangle := D_S(\xi) e^{\xi S^+} |S, -S\rangle, \tag{C1}$$

where S^+ is the raising operator of the angular momentum algebra su(2) generated by S_z, $S_x = (S^+ + S^-)/2$, and $S_y = (S^+ - S^-)/2i$ which fulfill the standard commutators

$$[S^z, S^\pm] = \pm S^\pm 2, \quad [S^+, S^-] = 2S_z. \tag{C2}$$

$D_S(\xi) \doteq 1/(1+|\xi|^2)^S$ represents a normalizing factor, whereas $|S, -S\rangle$, the so-called maximum weight vector, satisfies the equation $S^-|S,-S\rangle = 0$. The action of $S^\pm$

$$S^\pm |S,m\rangle = \sqrt{(S \mp m)(S \pm m + 1)}\, |S, m \pm 1\rangle$$

is represented on the standard basis $\{|S,m\rangle; |m| < S\}$ the vectors of which obey the secular equation $S^z|S,m\rangle = m|S,m\rangle$. Making explicit the action of S^+ in Eq. (C1) supplies the spanned form

$$|\xi\rangle = D_S(\xi) \sum_{m=-S}^{S} C_m(S) \xi^{m-S} |S,m\rangle$$

of $|\xi\rangle$, with $C_m(S) \doteq \sqrt{(2S)!/(S-m)!(S+m)!}$. Based on such a formula, one is able to calculate the expectation values

$$L_z = \langle S^z \rangle = S \frac{|\xi|^2 - 1}{|\xi|^2 + 1}, \tag{C3}$$

$$L^* = \langle S^+ \rangle = S \frac{2\xi}{|\xi|^2 + 1}, \tag{C4}$$

where $\langle \bullet \rangle \doteq \langle \xi | \bullet | \xi \rangle$, and therefore to reconstruct the sphere equation $(L^z)^2 + (L^x)^2 + (L^y)^2 = S^2$, where $L = L^x - iL^y = (L^*)^*$ for the classic spin (L^x, L^y, L^z). Such an equation, in turn, can be viewed as the classic counterpart of the (quantum) Casimir equation $(S^z)^2 + (S^x)^2 + (S^y)^2 = S(S+1)$ for (S^x, S^y, S^z) in terms of the SCS picture and illustrates the semiclassical content thereof. Upon introducing the macroscopic wave function

$$|\Phi\rangle \doteq e^{i\mathcal{S}/\hbar} |\xi\rangle, \tag{C5}$$

where the trial state $|\xi\rangle \cdot = \otimes_i |\xi_i\rangle$ and $|\xi_i\rangle$ is the SCS for the ith spin (S_i^x, S_i^y, S_i^z), then one easily constructs the TDVP semiclassical dynamics relative to spin Hamiltonian (3)

$$H_S = -h \sum_i (S_i^z + S) + U \sum_j (S_j^z + S)(S_j^z + S - 1)$$
$$- \frac{E_S}{2} \sum_{\langle i,j \rangle} (S_i^+ S_j^- + S_j^+ S_i^-),$$

(now assumed to be constituted by spins with $S > 1/2$), by proceeding along the same lines as Appendix A. The resulting Hamiltonian $\mathcal{H}_S := \langle \xi | H_S | \xi \rangle$ reads

$$\mathcal{H}_S = -h_* \sum_i L_i^z + U \sum_i [(1 - 1/2S)(L_i^z)^2 + S/2]$$
$$- \sum_i S[US + h_*] - \frac{E_S}{2} \sum_{\langle i,j \rangle} (L_i^* L_j + L_j^* L_i), \tag{C6}$$

where $h_* = h - U(2S-1)$, and we have used the fact that, via a nontrivial calculation, one finds $\langle (S^z)^2 \rangle = (1 - 1/2S)(L_i^z)^2 + S/2$. Furthermore, stationarizing the action $\mathcal{S} = \int dt \langle \xi | (i\hbar \partial_t - H_S) | \xi \rangle$ provides the equations of motion for the variables L_i^*, L_i [see Eqs. (5)], where L_i^z is depending on

L_i, L_i^* via the constraint introduced above for the spin expectation value components $(L_i^z)^2+|L_i|^2\equiv S^2$. Once the brackets

$$\{A,B\}=\sum_j \frac{(1+|\xi_j|^2)^2}{2Si\hbar}\left[\frac{\partial A}{\partial \xi_j}\frac{\partial B}{\partial \xi_j^*}-\frac{\partial B}{\partial \xi_j}\frac{\partial A}{\partial \xi_j^*}\right] \quad \text{(C7)}$$

have been defined, one can easily check that $\{L_j^*,L_j\}=2L_j^z/i\hbar$, $\{L_j^z,L_j^*\}=L_j^*/i\hbar$, and $\{L_j^z,L_j\}=-L_j/i\hbar$ consistently with Eq. (C2), while the dynamical equations issued from the TDVP can be recovered as well from $\mathcal{H}_S$. Equivalently, the alternative form of the above Lie-Poisson brackets

$$\{A,B\}=\frac{1}{\hbar}\sum_j\left[\frac{\partial A}{\partial \phi_j}\frac{\partial B}{\partial L_j^z}-\frac{\partial B}{\partial \phi_j}\frac{\partial A}{\partial L_j^z}\right] \quad \text{(C8)}$$

can be reconstructed from Eq. (C7) when expressing L_i's as

$$L_i=\sqrt{S^2-(L_i^z)^2}e^{i\phi_i} \quad \text{(C9)}$$

through the action-angle variables ϕ_i, L_i^z. This fact states at the classical level the equivalence between the HPR and the VR introduced in Sec. III.

APPENDIX D: LOCAL PHASE DYNAMICS OF THE SHM HAMILTONIAN

This appendix is devoted to calculating explicitly the form assumed by the spin Hamiltonian in the proximity of the ground-state configuration in order to show how weakly excited states mimic the dynamics of the (classic) phase model. Upon recalling that the ground-state configuration is characterized by

$$\mathcal{L}_0\equiv h^*/(2U+qE_S), \quad \phi_i=\phi_j,$$

at each site j, considering the approximation

$$L_jL_i^*+L_iL_j^*\simeq 2g\cos(\phi_i-\phi_j)\times\left[1-\frac{\mathcal{L}_0}{g}(P_i+P_j)-f(P_i,P_j)\right],$$

where $P_j=L_j^z-\mathcal{L}_0$, $g=S^2-\mathcal{L}_0^2$, and

$$f(P_i,P_j)\equiv\left[\frac{\mathcal{L}_0^2}{2g^2}(P_i-P_j)^2+\frac{P_i^2+P_j^2}{2g}\right],$$

leads to rewriting spin Hamiltonian (4) as

$$\mathcal{H}_S\simeq C+\sum_i (UP_i^2+U\mathcal{L}_0^2-h_*\mathcal{L}_0) - gE_S\sum_{\langle i,j\rangle} f(P_i,P_j)-gE_S\sum_{\langle i,j\rangle}\cos(\phi_j-\phi_i). \quad \text{(D1)}$$

Decoupling $f(P_i,P_j)$ from the cosine term in the latter formula relies on the fact that $(\phi_j-\phi_i)^2\times f(P_i,P_j)$ is fourth order. The resulting model exhibits the QPM structure even if, within the present approximation scheme, the condition $|P_j|\ll\mathcal{L}_0$ only concerns the spin dynamics. The geometry of the sphere (the spin configuration space) is involved instead when one imposes $\beta=|m|/S\ll 1$ (m is the quantum number corresponding to $\mathcal{L}_0$) in order to make explicit the (local) cylinderlike geometry characterizing the QPM in the equatorial region.

[1] *Proceedings of the NATO Advanced Resarch Workshop on Coherence in Superconducting Networks*, edited by J.E. Mooij and G. Schön [Physica B **152** (1988)]; A. van Oudenaarden and J.E. Mooij, Phys. Rev. Lett. **76**, 4947 (1996); *Proceedings of the Conference on Macroscopic Quantum Phenomena and Coherence in Superconducting Networks*, edited by C. Giovannella and M. Tinkham (World Scientific, Singapore, 1995).

[2] B.G. Orr, H.M. Jaeger, A.M. Goldman, and C.G. Kuper, Phys. Rev. Lett. **56**, 378 (1986); H.M. Jaeger, D.B. Haviland, B.G. Orr, and A.M. Goldman, Phys. Rev. B **40**, 182 (1989).

[3] D.B. Haviland, Y. Liu, and A.M. Goldman, Phys. Rev. Lett. **62**, 2180 (1989); A.F. Hebard and M.A. Paalanen, *ibid.* **30**, 4063 (1984).

[4] M.A. Paalanen, A.F. Hebard, and R.R. Ruel, Phys. Rev. Lett. **69**, 1604 (1992).

[5] A justification of this picture comes from the renormalization-group calculations in T. Giamarchi and H.J. Schulz, Phys. Rev. B **37**, 325 (1988), where it is proved that the universality classes of the global superconducting transition of attracting electrons and of the superfluid transition of disordered bosons are identical.

[6] K.B. Efetov, Zh. Éksp. Teor. Fiz. **78**, 2017 (1980) [Sov. Phys. JETP **51**, 1015 (1980)]; S. Doniach, Phys. Rev. B **24**, 5063 (1981); R. Fazio and G. Schön, *ibid.* **43**, 5307 (1991).

[7] M.P.A. Fisher, B.P. Weichman, G. Grinstein, and D.S. Fisher, Phys. Rev. B **40**, 546 (1989).

[8] L.J. Geerligs, M. Peters, L.E.M. de Groot, A. Verbruggen, and J.E. Mooij, Phys. Rev. Lett. **6**, 326 (1989); H.S.J. van der Zant, L.J. Geerligs, and J.E. Mooij, Europhys. Lett. **19**, 541 (1992); C.D. Chen, P. Delsing, D.B. Haviland, Y. Harada, and T. Claeson, Phys. Rev. B **50**, 3959 (1995).

[9] The competition between the quantum fluctuation of n_i and Φ_i has a link with the energetic competition between the Coulomb and kinetic energies: the hopping processes, which tend to delocalize the particles, induce fluctuations of n_j thus reducing phase's fluctuations, and favoring the macroscopic phase coherence. On the contrary, a finite electrostatic energy tends to localize bosons, reduces the bosons number fluctuations, and consistently prompts strong fluctuations of Φ_j's at each site.

[10] L. Amico and V. Penna, Phys. Rev. Lett. **80**, 2189 (1998).

[11] We note how the set of z_j corresponds to the lattice version of the order-parameter field used in the standard scalar field theories for superfluidity. In this respect the slow part of z_j indeed should represent the order-parameter field of a superfluid medium when the contributions relative to small time scale are negligible (Ref. 37). In fact, the usual canonical conjugation between the phase of the superconducting order parameter and the total particle number N (see Ref. 12) is inherited naturally by the TDVP ef-

fective theory of the BHM. In this picture, in fact, the low-temperature dynamics is dominated by the z_j phases which is the condition whereby showing that the effective action (the phase of the medium wave functions) is canonically conjugated to N.

[12] D.R. Tilley and J. Tilley, *Superfluidity and Superconductivity* (Adam Hilger, Bristol, 1986).

[13] W. Krauth and N. Trivedi, Europhys. Lett. **14**, 627 (1991); W. Krauth, N. Trivedi, and D. Ceperley, Phys. Rev. Lett. **67**, 2307 (1991); R.T. Scalettar, G.G. Batrouni, and G.T. Zimanyi, *ibid.* **66**, 3144 (1991); P. Niyaz, R.T. Scalettar, C.Y. Fong, and G.G. Batrouni, Phys. Rev. B **44**, 7143 (1991); G.G. Batrouni and R.T. Scalettar, *ibid.* **46**, 9051 (1992).

[14] J.K. Freericks and H. Monien, Europhys. Lett. **26**, 545 (1993); Phys. Rev. B **53**, 2691 (1996); T.D. Kühner and H. Monien, Phys. Rev. B **58**, R14 741 (1998); N. Estner and H. Monien, cond-mat/9807033 (unpublished); cond-mat/9905367 (unpublished).

[15] Such models belong to the same universality class [see M.P.A. Fisher and G. Grinstein, Phys. Rev. Lett. **60**, 208 (1988)]; outside the phase boundaries characterizing the phase transition, they describe different physics.

[16] P. Carruthers and M.M. Nieto, Rev. Mod. Phys. **40**, 411 (1968); D.A. Dubin, M.A. Hennings, and T.B. Smith, Int. J. Mod. Phys. B **9**, 2597 (1995).

[17] L. Amico and V. Penna (unpublished).

[18] A. Montorsi and V. Penna, Phys. Rev. B **55**, 8226 (1997).

[19] D.S. Rokhsar and B.G. Kotliar, Phys. Rev. B **44**, 10 328 (1991); W. Krauth, M. Caffarel, and J.-P. Bouchard, *ibid.* **45**, 3137 (1992).

[20] A. van Otterlo, K-H. Wagenblast, R. Baltin, C. Bruder, R. Fazio, and G.G. Schön, Phys. Rev. B **52**, 16 176 (1995).

[21] R. Baltin and K–H. Wagenblast, cond-mat/9705261 (unpublished).

[22] We could define a Hermitian phase operator Φ, but it would not canonically conjugated to n.

[23] K.S. Liu and M.E. Fisher, J. Low Temp. Phys. **10**, 655 (1973).

[24] H Matsuda and T. Tsuneto, Prog. Theor. Phys. Suppl. **46**, 411 (1970).

[25] W.-M. Zhang, D.H. Feng, and R. Gilmore, Rev. Mod. Phys. **62**, 867 (1990).

[26] T. Fukui and Y. Tsue, Prog. Theor. Phys. **87**, 627 (1992).

[27] A. Inomata, H. Kuratsuji, and C.C. Gerry, *Path Integral and Coherent States of SU(2) and SU(1,1)* (World Scientific, Singapore, 1992).

[28] Equation (B16) has been found by M.P.A. Fisher *et al.* in Ref. 7 by using general scaling arguments.

[29] K. Sheshadri, H.R. Krishnamurty, R. Pandit, and T.V. Ramakrishnan, Europhys. Lett. **22**, 257 (1992).

[30] A. Montorsi, M. Rasetti, and A. Solomon, Phys. Rev. Lett. **59**, 2243 (1987).

[31] R. Gilmore, *Lie Groups, Lie Algebras, and Some of Their Applications* (Wiley, New York, 1974).

[32] L. Amico, cond-mat/0002410 (unpublished).

[33] In the limit, the spin projection along z follows its representation.

[34] V. Barone, V. Penna, and P. Sodano, Int. J. Mod. Phys. B **21**, 3525 (1992).

[35] D. C. Mattis, *The Theory of Magnetism: Statics and Dynamics* (Springer-Verlag, Berlin, 1981).

[36] In the limit, the z-spin's projection is kept finite. Only after the limit, S_i^z range on a infinite interval.

[37] V. Ambegaokar, B.I. Halperin, D.R. Nelson, and E.D. Siggia, Phys. Rev. B **21**, 1806 (1980).